Assessment of SIMMER-III code in predicting Water Cooled Lithium Lead Breeding Blanket "in-box-Loss Of Coolant Accident"

Marica Eboli[a]*, Nicola Forgione[b], Alessandro Del Nevo[a]

[a] *ENEA FSN-ING-SIS, C.R. Brasimone, 40032 Camugnano (BO), Italy*
[b] *DICI, University of Pisa, Largo Lucio Lazzarino 2, 56122 Pisa, Italy*

The in-box Loss of Coolant Accident is a major safety concern for the Water Cooled Lithium Lead Breeding Blanket design. SIMMER-III code has been modified by University of Pisa and ENEA C.R. Brasimone to perform deterministic safety investigation of such accidental scenario. Thanks these modifications, this version of the code has unique features for dealing with the PbLi water reaction related phenomena. The reliability of the code requires a systematic validation activity, carried out applying a standard methodology based on a three-steps procedure and through qualitative and quantitative evaluations. The methodology was applied to the LIFUS5 campaign. Post-test analyses highlighted open issues of test execution and of experimental data, as well as code limitations and capabilities. Nevertheless, the modified version of SIMMER-III code for fusion application is able to predict the relevant thermal-hydraulic phenomena during PbLi/water interaction.

Keywords: SIMMER, Chemical Reaction, Deterministic Safety Analysis, WCLL Breeding Blanket, Code Validation.

1. Introduction

The Water Cooled Lithium Lead (WCLL) is one of the candidate breeding blanket concepts currently under investigation for EU DEMO ([1], [2]) and one of the European Test Blanket Module (TBM) concepts that will be qualified in the ITER reactor ([3]). The postulated interaction between lithium-lead and water following by a water tube rupture in the breeding zone is a major safety concern for this component which should be carefully investigated [4]. Indeed, the interaction leads to:

1. pressure transient governed by mixing and pressurization , with pressure which might exceed the design limits,
2. chemical reaction contributing to pressure and temperature increases and which might generate a more severe system condition,
3. hydrogen production that might represent a potential source of energy.

The possible consequences of a postulated PbLi/water interaction due to in-box Loss Of Coolant Accident (LOCA) can be prevented by adequate WCLL components design (e.g. the adoption of double wall tubes, detection systems, etc…) and mitigated by active or passive systems. Nevertheless, it is fundamental to evaluate and predict the main thermo-hydraulic parameters which might affect the accidental scenario (i.e. pressure, temperature, hydrogen generation) in order to assure the mechanical resistance of the component itself, or in the worst case, to avoid jeopardizing the entire system.

The definition of the approach (Fig. 1) for addressing the in-box LOCA derives from the review of studies and activities performed in the past, the knowledge of phenomena and processes occurring during lithium-lead water interaction and chemical reaction, and the status of codes capabilities in predicting the transient [4], i.e. blue box in Fig. 1.

The review pointed out the need for a predictive tool for a reliable analysis of the consequences of the "in box LOCA" [5]. This numerical code is required to support the design of the breeding blanket, the safety and the design of the experimental campaign required for the component qualification. SIMMER code was found to be the most promising code for the analysis of such transient because of the possibility to deal with two working fluids in the same mesh cell. SIMMER code was modified (i.e. red box) to model the exothermic chemical reaction between water and lithium-lead, generating oxides and hydrogen. Then, the verification phase was successfully demonstrated [6].

Following the verification, the validation phase is a fundamental step to demonstrate the reliability of qualified system code for the deterministic safety analysis of WCLL BB in-box LOCA. A validation procedure was set-up and applied for the assessment of SIMMER code [7] against available experiments, as discussed in the present manuscript.

According to the R&D plan, the activity will continue with the design and follow up of an experimental campaign to be executed in LIFUS5/Mod3 facility ([8], [9]), specifically designed for SIMMER code validation purposes (i.e. green box).

Once SIMMER code will be validated using Separate Effect Test experiments ([10], [11]), the R&D plan envisages the experimental qualification of the WCLL BB and connected systems and the validation of SIMMER code against Integral Test Facility experiments [12] and the qualification of the safety analysis

*author's email: marica.eboli@enea.it

procedure (i.e. violet box). This involves the set-up of a chain of codes, including coupling where needed, and of the procedure for their application, as depicted in the yellow box. Pioneering activity are described in Refs. [13], [14].

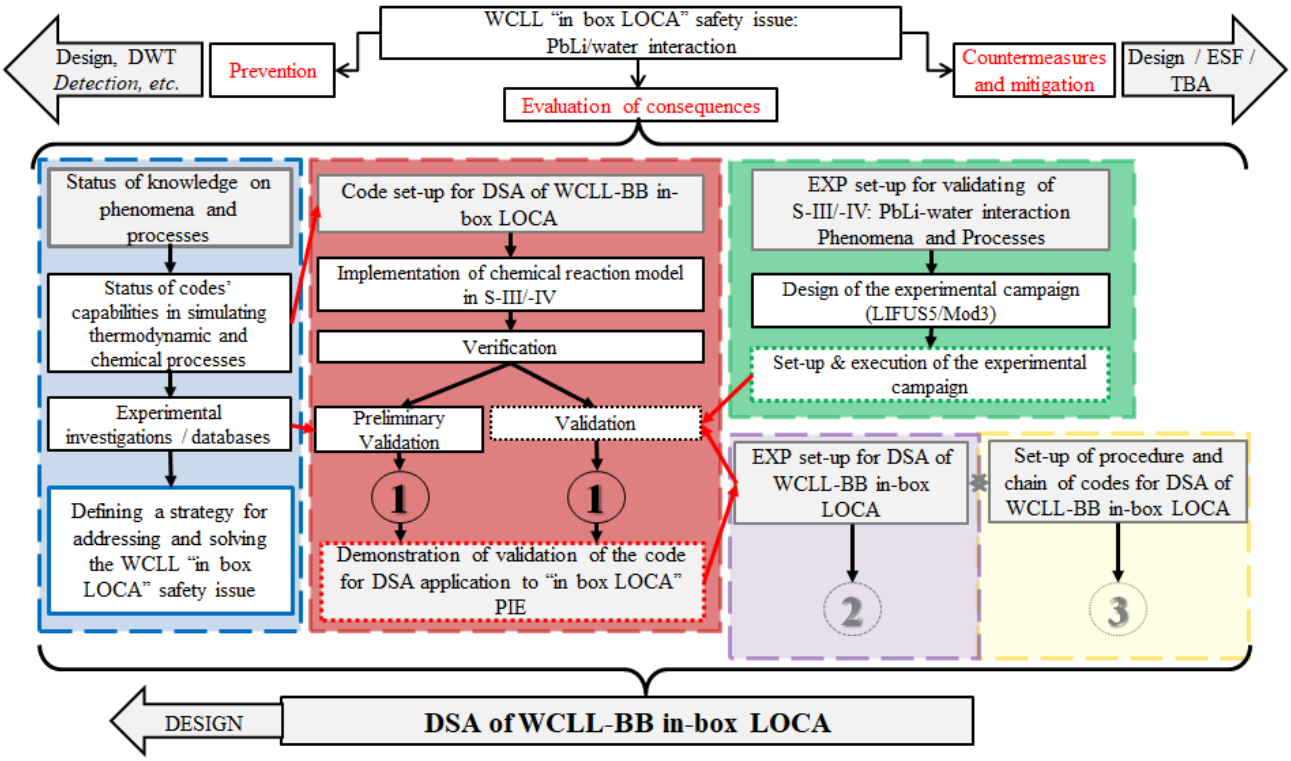

Fig. 1. Flowchart of WCLL BB in-box LOCA safety issue approach.

2. Procedure for code validation

The paper presents the validation of the "SIMMER-III Ver. 3F Mod. 0.1", the version of SIMMER-III modified for fusion application, developed by implementing the PbLi/water chemical reaction model [6]. The activity was carried out by applying a standard methodology procedure [15], [16]. The flow chart of the procedure is shown in Fig. 2 and hereafter described.

The methodology starts with the development of the qualified nodalization input deck which depends on several aspects:

- Code models. The information is available by the user manual and by the guidelines for the use of the code. They take into account the specific models, limits and assumptions of the code;
- User experience and capability. The user's knowledge about the code is useful for the modeling phase;
- Facility geometry. The main geometrical dimensions of the facility are derived from the experimental database. This information should be derived from official document and traceability of each reference should be maintained.

Boundary and initial conditions of the considered experiment (i.e. input data for the reference calculation) may be changed within their uncertainty ranges in order to get the reference calculation; if a user's choice is introduced (e.g. changes in nodalization detail due to lack of experimental data, misinterpretation of test, deficiency of geometrical information), its validity and acceptability must be checked by repeating the nodalization qualification process.

Then, a three-step analysis [17], [18] is pursued as a part of the code assessment process:

1. Initial condition results at injection time;
2. Reference calculation results;
3. Results from sensitivity analyses.

Step 1 constitutes part of the assessment process being relevant for the characterization of the thermal-hydraulic conditions at the beginning of the experiment. The reference calculation results (step 2) are those achieved from the qualified nodalization. Sensitivity analyses (step 3) are carried out to demonstrate the robustness of the calculation, to characterize the reasons for possible discrepancies between measured and calculated trends that appear in the reference calculation, to optimize code results, user option choices, and to improve the understanding of experimental data.

The analysis of results is based on a comprehensive comparison between measured and calculated trends or values, performed through 1) qualitative engineering judgments, and 2) quantitative evaluation of calculated-experimental discrepancies, including the following steps:

a) analysis of code results and comparisons between experimental and calculated time trends on the basis of the selected variables;
b) evaluation of quantities relevant for the assessment of phenomena/processes and for the safety [16], including the resulting sequence of main events;
c) evaluation of the accuracy based on selected figures of merit [19]-[23].

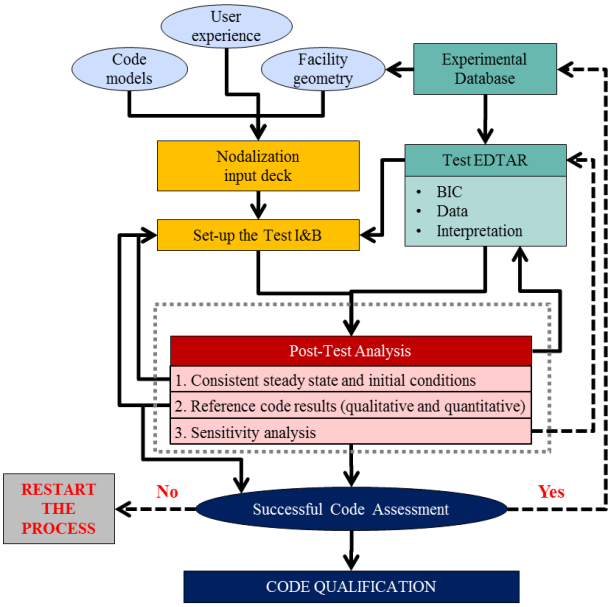

Fig. 2. Methodology for SIMMER code validation.

The qualitative accuracy evaluation is based upon a procedure consisting in the identification of phenomenological windows and of the RTA (relevant thermal-hydraulic aspects) [16]. It essentially derives from a visual observation of the experimental and predicted trends. Then, the parameters characterizing the RTA are quantified, giving information about the discrepancy between experimental and calculated results, according to the following qualitative indicators:

- Excellent (E): the calculation result lies within the uncertainty band of experimental data. The code predicts qualitatively and quantitatively the parameter;
- Reasonable (R): the calculation result shows only correct behavior and trends. The code predicts qualitatively but not quantitatively the parameter;
- Minimal (M): the calculation result lies within experimental data uncertainty band and sometimes does not have correct trends. The code does not predict the parameter, but the reason is understood and predictable;
- Unqualified (U): the calculation result does not show correct trend and behavior, reasons are unknown and unpredictable. The code does not predict the parameter and the reason is not understood.

The qualitative analysis is a prerequisite for the application of the quantitative analysis to avoid misinterpretation due to compensation of errors. Quantitative accuracy evaluation can be defined as a systematic analysis of the deviation of the predicted target variables with respect to the corresponding measured values [21], [22]. Therefore, it plays a relevant role to quantify the accuracy of a code, thus the reliability and the capability in predicting parameters relevant to safety.

The statistic approach is based on time-averaging deviations of selected statistical parameters [19]. The starting point is the definition of the following equation:

$$DEV1_{i,t} = c_{i,t} - e_{i,t} \quad (1)$$

which is simply the difference between the calculated and the experimental values (c and e, respectively), for each location i and for each time value t. Both the calculated and the measured values must be "aligned" on the same time vector (usually this is not the case because the frequencies of experimental data acquisition and code results are most likely to be different).

Once the DEV1 deviations have been calculated, they can be "integrated" over the specified time interval using the following equations. In this way, it is possible to obtain three deviations DEV2: DEV2_SIGN, which represents the cumulative error and it is positive if the local perturbation has been over-predicted (and vice versa); DEV2_ABS, which is the sum of the absolute deviations (always non-negative) and DEV2_RMS, which accounts for the root mean square deviation and enhances the contribution due to the large deviations.

$$DEV2\_SIGN_i = \frac{1}{t_N - t_0} \cdot \sum_{k=1}^{N} DEV1_{i,t} \cdot (t_k - t_{k-1}) \quad (2)$$

$$DEV2\_ABS_i = \frac{1}{t_N - t_0} \cdot \sum_{k=1}^{N} |DEV1_{i,t}| \cdot (t_k - t_{k-1}) \quad (3)$$

$$DEV2\_RMS_i = \sqrt{\frac{1}{t_N - t_0} \cdot \sum_{k=1}^{N} (DEV1_{i,t})^2 \cdot (t_k - t_{k-1})} \quad (4)$$

Another methodology suitable to quantify code accuracy (FFTBM = Fast Fourier Transform Based Method approach) was developed at the University of Pisa [20], [23]. It consists of performing a discrete Fourier transform on both the experimental and the calculated time history of a given key parameter (over a specified time interval, and filtering the frequencies above a specified threshold), then comparing the resulting amplitudes in the space of frequencies. In particular, considering the experimental signal $F_{exp}(t)$, the calculated signal $F_{calc}(t)$, and the error function, $\Delta F(t) = F_{calc}(t) - F_{exp}(t)$, the method defines two values characterizing each calculation:

- A dimensionless average amplitude

$$AA = \frac{\sum_{n=0}^{2m} |\tilde{\Delta}F(f_n)|}{\sum_{n=0}^{2m} \tilde{F}_{exp}(f_n)} \quad (5)$$

- A weighted frequency

$$WF = \frac{\sum_{n=0}^{2m} |\tilde{\Delta}F(f_n)| \cdot f_n}{\sum_{n=0}^{2m} \tilde{\Delta}F(f_n)} \quad (6)$$

where f_n is the discrete frequency $n = 0,1,\ldots,2^m$, and m is the exponent defining the number of points. The most significant information is given by the factor AA, which represents the relative magnitude of the discrepancy deriving from the comparison between the addressed calculation and the corresponding

experimental trend (AA=1 means a calculation affected by a 100% of error). The WF factor characterizes the kind of error, because its value emphasizes whether the error has more relevance at low (small value of WF) or high frequency ones (large value of WF). The higher is the weighted frequency, the more relevant is the contribution of the high frequencies to the average amplitude. The two resulting factors AA and WF represent a quantification of the code results accuracy. However, they acquire a practical and understandable meaning only when they are compared with some analogous factors (e.g. corresponding results proceeding from different calculations and reference values). For instance they can be compared with the same quantities coming from different calculations (for a code-to-code comparison) or with reference values (e.g. "acceptability thresholds").

Then, sensitivity analyses are performed in order to investigate the robustness of the code results and to evaluate the relevance of selected parameters and/or user choices (Ref. [24]) on the results.

When the results of the post-test analyses are positive and fulfill both qualitative and quantitative accuracy evaluations, the validation process can proceed with another test without modifications in the nodalization.

This methodology for code assessment was applied to validate SIMMER-III code against the experimental campaign on LIFUS5 performed during the first years of the 2000 decade at ENEA CR Brasimone [25], [26] and hereafter discussed.

3. Description of LIFUS5 experiments

3.1 Facility description

LIFUS5 facility ([25], [26]) was designed and operated at ENEA CR Brasimone to experimentally investigate the consequences of LOCA accidents in liquid metal pools. Fig. 3 shows the P&ID of the facility. It mainly consisted of:

- Reaction vessel S1 with the water injection device. S1 was the vessel where the reaction between the liquid metal and the pressurized water took place. The vessel was divided by two AISI 316 plates into 4 sectors simulating the toroidal stiffener that, in the WCLL BB reference design [27], acted as structural constraints and liquid metal flow separator. In one of these sectors, a mock-up of U shaped cooling tubes, as foreseen in previous design of the WCLL BB for DEMO, is located The mock-up consisted of ten U tubes of 16.5 mm of external diameter and about 0.65 m in length. This pipe bundle was located in one out of four sectors, in which the vessel was divided by two AISI 316 plates. The functionality of the mock-up was to investigate the possible structural consequences of pressure wave propagation during a postulated LOCA.
- Expansion vessel S5 connected to the reaction vessel through four expansion tubes and a 3" pipe;
- Pressurized water vessel S2 connected to S1 by the injection line and valves V14 and V4;
- Safety vessel S3;
- Liquid PbLi storage vessel S4.

The water injection device was placed in the bottom of S1 below the tube bank sector. It had an orifice diameter of 4 mm and a protective cap which was supposed to break at 155 bar. Several pressure transducers (PT) and thermocouples were placed both in S1 and in the expansion vessel S5 to follow the pressure and temperature evolution during the metal-water interaction.

3.2 Tests description and open issues

Before the execution of a test, vacuum was generated between the valve V14 and the water injector. At the start of the test, valve V14 opened and hot pressurized water was discharged from the water tank S2 to S1 through the injection line. The water injection pressure was fixed and kept as constant as possible through a pressurization of the vessel S2. Then, the injection was interrupted closing the valve. The main operating conditions of each Test# are summarized in Table 2. On the basis of the review of available documents and of the validation activity ([7], [25], [26], [28]), the knowledge of the execution of the experiment is affected by uncertain data in relation to:

- Layout of the injector device and relative position in respect to the U-tube mock-up.
- Mass of water injected, because no specific instrumentation was available to quantify this parameter: it was evaluated by the experimentalists a posteriori.
- Position of PT3. From the original drawing, PT3 was installed in the ascendant pipe of the vacuum line. Therefore, it is possible that the pressure recorded by PT3 was affected by vapor bubble formation, PbLi plugs, or PbLi drops which fall down and vaporize the water in the injection line, causing the increase of pressure recorded by the PT.

4. LIFUS5 SIMMER-III nodalization

4.1 Facility nodalization

The nodalization of LIFUS5 by SIMMER-III code [29] is developed in 2D cylindrically axisymmetric geometry (R-Z), despite the limitation of representing the asymmetries of LIFUS5 facility. In fact, the injection device and the tube bundle are not placed along the central axis of S1, but in one of the sectors limited by plates, while the expansion tubes are one for each sector. Therefore, assumptions were made in order to model this asymmetric layout. This implies that the user effect due to modeling choices and code options selections are relevant for the results of simulations. The nodalization set up for the reference calculation is shown in Fig. 4. It is constituted by 6 main parts:

- The injector device;
- The reaction vessel S1;
- The U-tube bundle mock-up;
- The expansion tubes;
- The 3" connecting pipe;

- The expansion vessel S5.

The geometrical domain is obtained by I = 11 radial and J = 47 axial mesh cells. Colors distinguish the different fluids, as set at the beginning of the transient (t = 0 s). Therefore, the PbLi is represented in red, the water in blue, the cover gas (and the hydrogen produced by the reaction) in white, and the non-calculation zones are highlighted by green mesh fence. The overall volume of the model is obtained rotating the 2D SIMMER domain along the central axis of symmetry. The reference mesh cells used for the analysis and the comparison with experimental data are highlighted in yellow and are (6,4), (6,7) and (6,10) for the pressure in the reaction vessel S1 and (5,47) for the pressure inside the expansion vessel S5. Considering the temperature, the nomenclature follow the same rationale, i.e. TLK1(5,47) means the PbLi temperature in radial mesh cell 5, axial mesh cell 47. The correspondence of main dimensions of LIFUS5 and SIMMER-III nodalization is reported in Table 1.

4.1.1 Reaction vessel

S1 vessel is modeled in the region I=1-11, J=1-18. The subdivision of the vessel in 4 identical sectors is modeled by virtual walls, which recreate two different concentric annuli. The virtual walls are located between I=6 and I=7, J=2-18. The first annulus represents the sector where the U-tube mock-up was installed. Its volume is ¼ of the total S1 volume. The second ring represents the other three sectors, with a volume of ¾ of the total one.

4.1.2 U-tube bundle mock-up

The U-tube mock-up is represented by steel structures located at I=4, I=5 and I=6. Axially, they cover J=4-18. In the radial cell I=4, four U-tubes mock-up are modeled, the closest to the injector. Then, eight tubes for each radial cell. The volume fraction of the structure is calculated dividing the total area of the tubes and the total area of the cell. The tube elbows above the injector is neglected.

4.1.3 Injector device

The injection line was horizontally installed and cannot be coherently modeled in an axisymmetric domain. Therefore, it was not modeled. There is no information or geometrical drawings about the exact position of the injector device towards the U-tube mock-up. The model of the injector is located at I=1-3, J=1-2. It has an orifice of 4 mm on the top, just below the injector cap. The dimension of the orifice is simulated by virtual walls, which reduce the diameter from ½'' to 4 mm.

4.1.4 Expansion tubes

The four cruciform pipes connecting S1 to S5 are not axisymmetric, therefore assumptions were made to model them. The expansion tube of the sector containing the mock-up is modeled by a central tube having the same inner diameter (11 mm), to preserve the flow area. This tube is located at I=1-2, J=19-27. The other three tubes are modeled by an annulus with the equivalent flow area. This region is located at I=9, J=19-28. Then, a ring models the horizontal tubes that connect the expansion tubes to the 3" pipe.

4.1.5 Three-inch connecting pipe

The 3" connecting pipe is modeled by a cylinder centered on the symmetry axis, located at I=1-4, J=28-31. The nodalization takes into account the real height and diameter of the component, maintaining the volume.

4.1.6 Expansion vessel

The expansion vessel S5 is modeled by a cylinder centered on the symmetry axis, located at I=1-5, J=32-47. The volume of 3" connecting pipe plus the S5 expansion vessel are preserved and equal to 10.1 liters.

4.2 Boundary and Initial Conditions

The reference calculations starts at t = 0 s when the valve V14 opens. The injector break-up is simulated by the virtual wall disappearing, which recreates the 4 mm orifice. The time at which the injector breaks-up depends on the experimental data of the single Test#.

The boundary conditions are applied at the injector device (I=1-3, J=1). In Tests#6-8 it is assumed to impose the pressure recorded by PT3, while in Tests#3-5 it is assumed a postulated time trend. Moreover, the temperature of the injected water, specified by the Test#, and the continuous water inflow are imposed at the same mesh cells. The initial conditions of pressure, temperature, filling level of lithium-lead in S1 and S5 are set coherently with the experimental data of each Test#.

The amount of injected water is calculated by SIMMER-III accordingly to pressure difference between the injector inlet and the reactor vessel. The flow is then controlled by the interaction phenomena between lithium-lead and water.

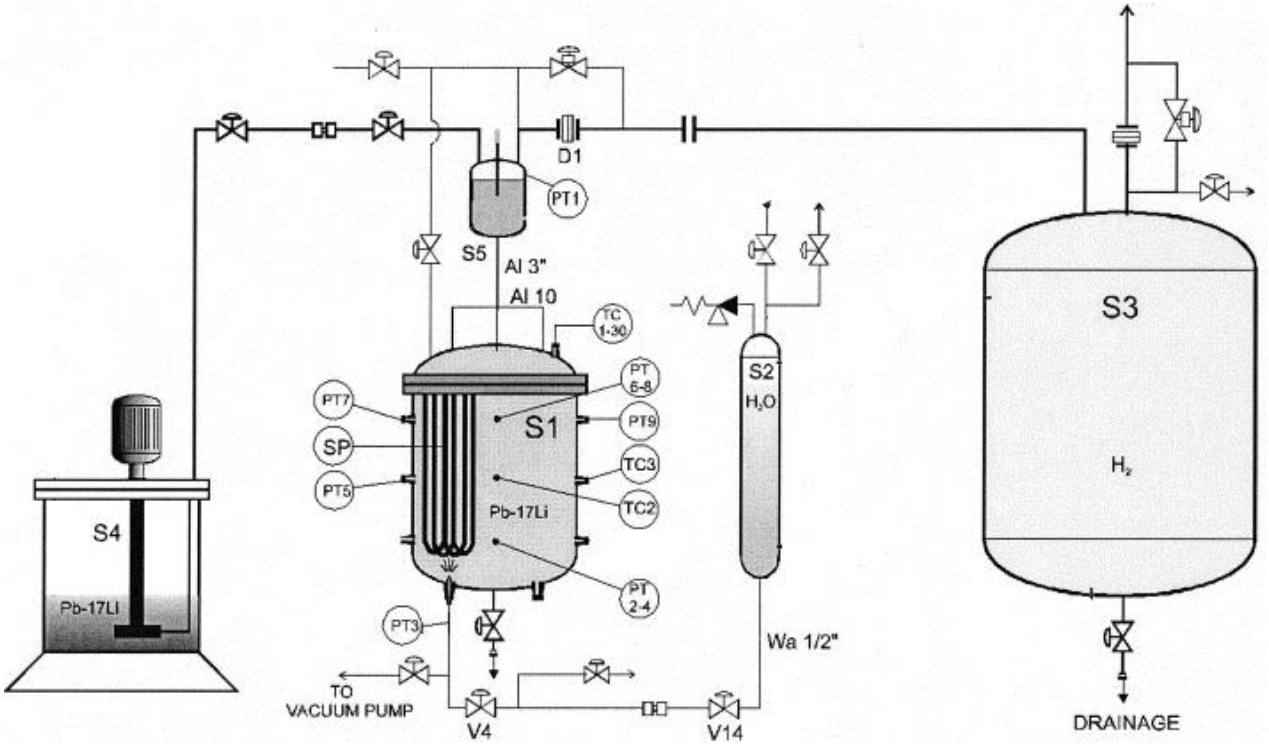

Fig. 3. P&ID of LIFUS5 facility.

Table 1. LIFUS5 reference model by SIMMER-III: correspondence of main dimensions.

		LIFUS5 modeling		**LIFUS5 facility**
Facility zone	*ID*	*cells*	*dimension*	*dimension*
S1	h [m]	1-18	0.775	0.780
	D [m]	1-11	0.420	0.42
	V [m^3]	-	0.107	0.1
Expansion Tubes	h [m]	19-27	0.505	0.264+0.235
	D ring [m]	1-2 9	0.011 2.95E-4	4x0.011
	A tot [m^2]	-	3.8E-4	3.80E-4
3" connecting pipe	h [m]	28-31	0.171(1)	0.189
	D [m]	1-4	0.07366	3" sch80
	V [m^3]	-	7.28E-4(2)	--
S5	h [m]	32-47	0.685(1)	0.794
	D [m]	1-5	0.101	6'' sch.160
	V [m^3]	-	9.35E-3(2)	0.0101
Mock-up Sector	h [m]	1-18	0.775	4x0.025
	D [m]	1-6	0.105	
	V [m^3]	-	0.027	
3 Sectors	h [m]	1-18	0.775	
	ring [m]	7-11	0.105	
	V [m^3]	-	0.08	
Injection device	h [m]	1-2	0.08	0.08
	D [m]	1-3	0.01388	½''
	D orifice [m]	1	0.004	0.004

(1) The heights of 3" connecting pipe and S5 vessel are modeled as compromise between volume and real design value.

(2) The sum of the volumes of S5 and 3" connecting pipe models the whole volume of 10.1 liter of the expansion vessel.

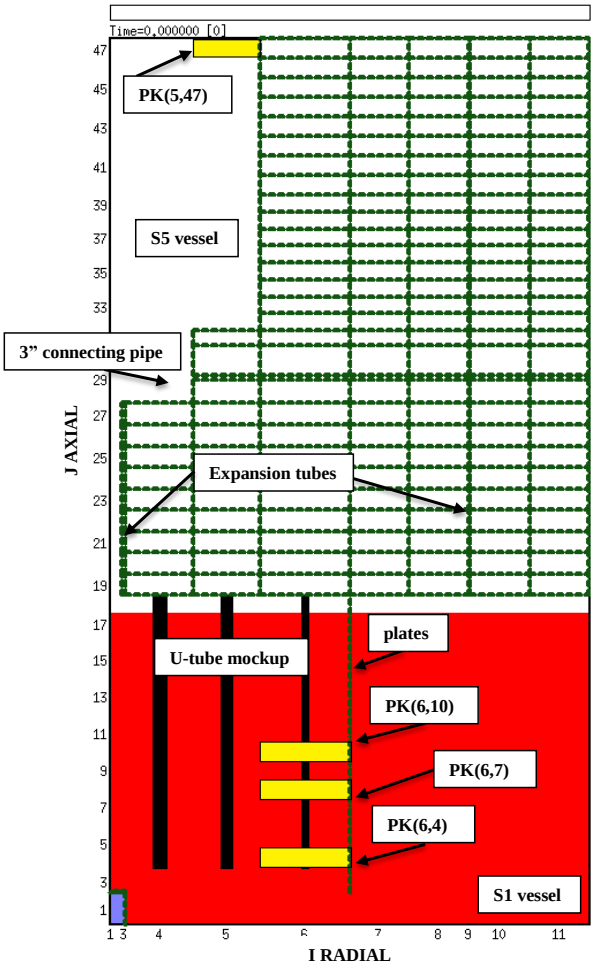

Fig. 4. SIMMER-III modeling of LIFUS5 facility and focus on reference mesh cells.

4.3 Modified input deck

The qualified nodalization was used in all the performed calculations with the exception of Test#3 (Ref. [7], [28], [30]). Moreover, in two sensitivity analyses (see Section 5.3) the nodalization was changed in order to investigate 1) the effect of the uncertainty in the geometrical data (i.e. relative position between injector and tube bundle), and 2) the user effect (i.e. nodalization approach and modeling choices):

- Run#7: the U-tube mock-up is represented by steel structures located in three rings at I=4, I=5 and I=6. Axially, they cover J=4-18. In ring 4, four U-tubes mock-up are modeled, the closest to the injector. Then, nine tubes at ring 5 and seven tubes at ring 6 are represented (identified by different colors in Fig. 5a). A simplified model of the curves which are responsible to broke the water jet, is implemented. It consist of SIMMER structures positioned at I=1-3, J=4 with a volume fraction that simulates a flow blockage of 99% directly above the injector, and 50% radially. A sketch of the nodalization is represented in Fig. 5a.
- Run#8: a different modeling of U-tube mock-up is adopted, in order to investigate the effect on the PbLi temperature. In this model, the width of radial mesh cells 4, 5 and 6 (and therefore the area of the rings obtained by rotating the mesh cells around the axis of symmetry) are calculated preserving the cross flow area of PbLi and the average distance of the tubes from the injector device. Then, the volume fraction of structures are imposed assuming two tubes in ring 4, six tubes in ring 5 and 12 tubes in ring 6 (identified by different colors in Fig. 5b). The simplified model of the curves which are responsible to break the water jet, is also modeled, positioned at I=1-3, J=4 with a volume fraction that simulates a flow blockage of 99% directly above the injector, and 50% radially.

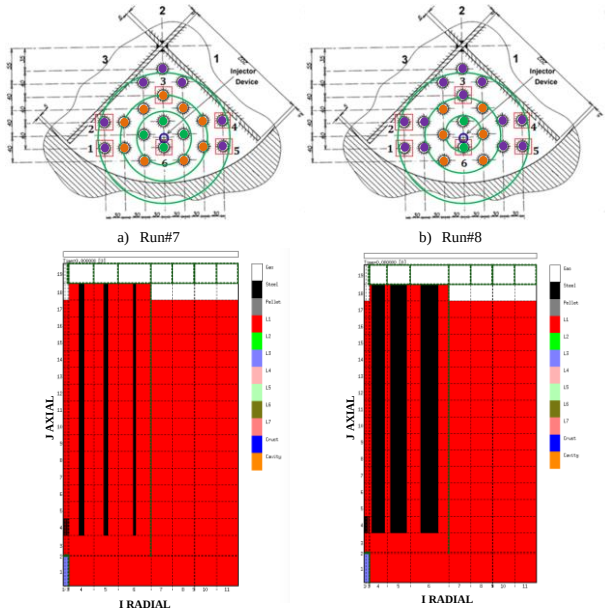

a) Run#7 b) Run#8

Fig. 5. Sketch of U-tube mock-up nodalization.

5. Post-tests analyses results

The code validation methodology was applied to all the Test# of LIFUS5 experimental campaign reported in Table 2. The obtained results are fully reported in Refs. [7], [30]-[35]. In the following, T#8 results are briefly described as sample application of the code validation methodology.

Table 2. LIFUS5 Test# operating conditions.

Parameter	T#3	T#4	T#5	T#6	T#7	T#8
PbLi Temperature [°C]	330	330	330	330	330	430
H_2O injection pressure [bar]	155	155	150	160	160	160
H_2O Temperature [°C]	295	325	265	320	320	320
Free volume in S5 (+S1) [liter]	5	5	4	10 (+7.5)	10 (+7.5)	10 (+7.5)
Amount of PbLi [liter]	105	105	106	92.5	92.5	92.5
Time of injection [s]	6	6	12	12	12	12

5.1. Initial conditions results

The step 1 of the three-step procedure is the initial conditions results predicted by the code. The SIMMER-III results at the time of valve opening (t = 0 s for the reference calculation) are reported in Table 3.

5.2. Reference calculation results

Step 2 focuses on the reference calculation results, performed through qualitative and quantitative accuracy evaluations. The qualitative accuracy evaluation here discussed is based on the identification of phenomenological windows (Table 5) and of the RTA (see Table 6 and Table 7), giving a judgment based on a visual observation of the experimental and predicted trends and based on the quantification of the discrepancy between experimental and calculated results. T#8 reference calculation transient can be divided into five phenomenological windows, previously identified by the analysis of the experimental data (Fig. 6 to Fig. 10).

Phase 0 [from onset of valve opening to 334 ms]: water injection line pressurization. As soon as the valve V14 opens, water starts to flow and to pressurize the pipeline upstream the injection cap. The design of the test specifies that the cap should be ruptured at the reference pressure (i.e. 160 bar). This implies that water at 320 °C should enter in S1, having a sub-cooling of about 27 °C. Actually, the pressure recorded by PT3 and in the reaction vessel S1 do not confirm this test procedure. The start of the transient (t = 0 s) is selected as the time of the V14 opening. Then, the time trend of pressure recorded by PT3 is imposed as BIC. At this time, the early rupture leads to the injection of water in two-phase conditions, since the temperature of water is

almost fixed at the test condition. The thermal-hydraulic conditions of water at the start of the injection calculated by SIMMER-III code are listed in Table 4.

Phase 1 *[from 334 ms to 680 ms]:* coolant flashing and reaction vessel pressurization, from injection cap rupture up to onset of S5 pressurization. The water injection and the flashing in the liquid metal cause a sudden steep pressurization in the reaction vessel. The first pressure peak calculated by the code and due to flashing of water inside the reaction vessel S1 is 7.9 bar and occurs at 336 ms (PK[6,4]) while the first peak recorded by PT7 is 4.7 bar and occurs at 337 ms. The calculated pressure trend during this phase agrees with the experimental results. However, there are some differences. In particular, the calculated pressure are slightly overestimated during the Phase 1 due to higher pressurization rate. Moreover, this phase ends earlier in the reference calculation in respect to the experimental trend due to an anticipated onset of S5 pressurization (Phase 1 calculated by the code ends at 530 ms against the 680 ms of the experiment). The difference in results are due to the gas flow which rises from the interaction zone through expansion tubes towards expansion vessel S5. SIMMER-III code predicts the start of the gas mass flow rate at about 490 ms. Likely, the behavior is anticipated in respect to the experiment, but no data are available for comparison. The reason of these discrepancies between experimental and calculated values during this Phase, and which affects all the transient, are caused by the jet fragmentation modeling (see sect. 5.3).

Phase 2 *[from 680 ms to 1530 ms]*: expansion vessel pressurization driven by connecting pipe layout, from S5 pressurization onset up to reaction and expansion vessels pressures equalization. The phase starts with the pressurization of the expansion vessel S5 due to the incoming mass flow rate of gases through the expansion tubes As already discussed in the previous phase, SIMMER code anticipates the pressurization trend. The start of S5 pressurization occurs at 530 ms against the experimental value of 680 ms. The calculated pressure of S1 vessel partially agrees with the experimental trends. Differences in the order of 20 bar occur, probably due to the imperfect knowledge of the boundary and initial conditions (temperature of the injected water, free gas volume in the system, see sect. 5.3). In the experiment, the second phenomenological phase ends at approximately 1530 ms, while the code predicts the end of Phase 2 with certain delay, at approximately 2100 ms, due to an overestimation of the S1 pressure. From this time on, pressures of reaction and expansion vessels follow a very similar evolution.

Phase 3 *[from 1530 ms to 11777 ms]*: reaction and expansion vessels pressures equilibrium, from pressures equalization up to valve closing signal. This phase can be further divided into two sub-phases: a) up to the equilibrium between the injection and the system, b) up to the valve closing signal. Once the reaction and expansion vessel pressures are equalized in the experiment, they are joined together as a unique system. The pressure continues to increase because of the hydrogen generation and the heat of the reaction which promotes the water evaporation. The calculated pressure trend during this phase is very similar to the experimental value, being the difference less than 5 bar. At about 2800 ms, both in the experiment and in the calculation, the system pressure reaches the equilibrium with the pressure recorded by PT3. Indeed, the experimental pressures are aligned (the differences are due to the pressure drops between injection line and S1 vessel), while the calculation shows that the pressures are perfectly overlapped.

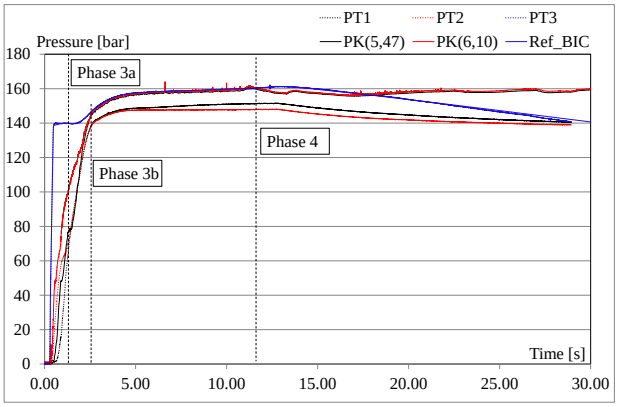

Fig. 6. T#8: pressure in S1 PK(6,10), in S5 PK(5,47), and imposed (Ref_BIC), and comparison with experimental data (PT).

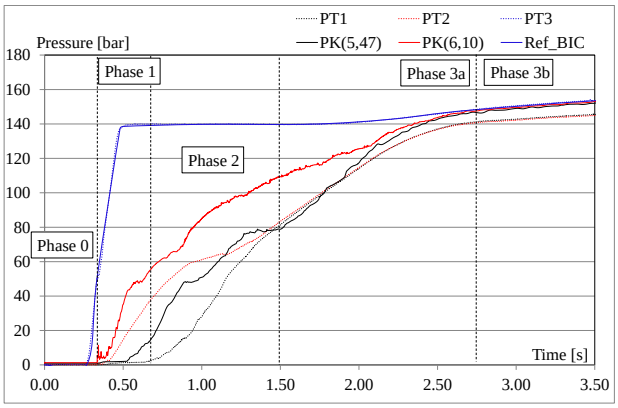

Fig. 7. T#8: pressure in S1 PK(6,10), in S5 PK(5,47), and imposed (Ref_BIC), and comparison with experimental data (PT) [zoom 0-3.5 s].

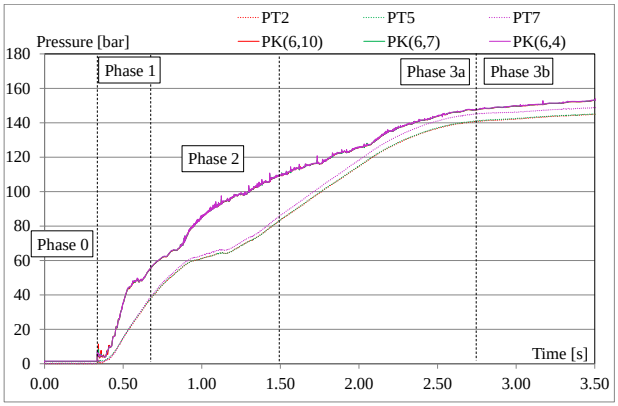

Fig. 8. T#8: pressure in S1 at different level PK(I=6, J=4-7-10), and comparison with experimental data (PT) [zoom 0-3.5 s].

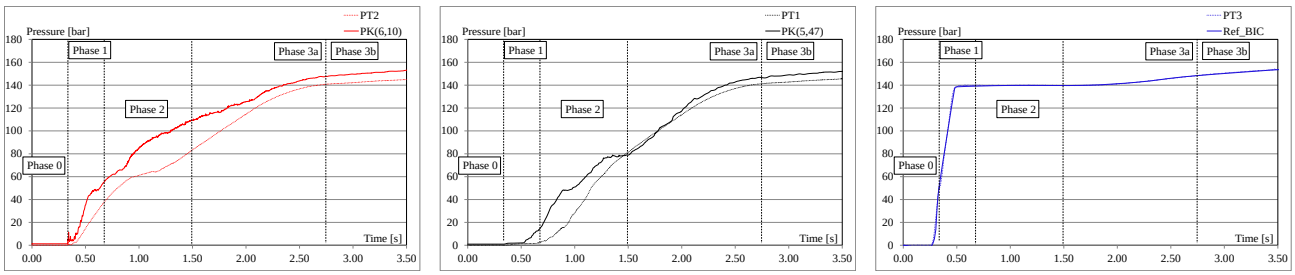

Fig. 9. T#8: pressure in S1 (left), S5 (center) and imposed (right), and comparison with experimental data (PT) [zoom 0-3.5 s].

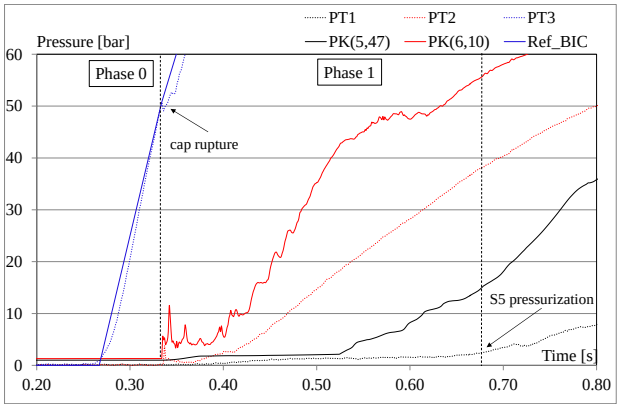

Fig. 10. T#8: pressure in S1 PK(6,10), in S5 PK(5,47), and imposed (Ref_BIC), and comparison with experimental data (PT) [zoom 0.2-0.8 s].

This behavior (S1 pressure follows the pressure imposed at the injector device) is due to the specific modeling choices and assumptions. Indeed, since geometrical features of the injection line and valve characteristics are missed, and due to code modeling simplification, the nodalization of the line from S2 water tank to S1 reaction vessel was not possible. Therefore, it was necessary to impose the pressure recorded by PT3 directly at the injector device. Imposing this pressure as BIC, the pressure in the reaction vessel calculated by the code follows this trend, and the code slightly over-predicts the pressure trend. At 4100 ms, the experiment shows that the pressure in the system (S1+S5) remains constant. This is a clear evidence that the pressure in the system is equalized with respect to the injection systems (S2 water tank and Argon cylinder). Phase 3 ends when the closing valve signal is generated at time 11777 ms.

Phase 4 *[from 11777 ms to EoT]*: system pressure stabilization, from valve closing signal to the EoT. During this phase the injection valve is closed and the parameters are stabilized. The pressures are almost constant in the simulation at 160 bar and decrease in the experiment (from 152 bar to 142 bar) with a rate of -0.57 bar/s due to temperature redistribution in the system (the overall system is at constant volume).

From a qualitative analysis of the transient, SIMMER code reasonably predicts the experimental temperature trends. Indeed, the code correctly predicts the zones where the temperatures are higher, i.e. the expansion vessel (Fig. 11) and the zone 1 of the mock-up (Fig. 12). The maximum temperatures occurring during the experiment are 450 °C (TC10 arrayed as depicted in Fig. 12 on the bottom right) and 473 °C recorded in S5 at 3270 ms. The calculated maximum values are 542 °C at 3816 ms in the expansion vessel (followed by two other peaks at 552 °C and 567 °C), and 506 °C at 517 ms in the reaction zone 1.

During the experiments, a cooling effect was encountered due to the injection of subcooled water which decreases the PbLi temperature up to the minimum value of 204 °C (at time 511 ms), see Fig. 13. SIMMER-III predicts a value of 235 °C at time 373 ms and at 478 ms (the minimum temperature predicted by the code is the PbLi melting point). This discrepancy could be explained considering the modeling of the U-tube geometry and of the water jet fragmentation. Indeed, the absence of the U-tube curves in the model improves the transport of the water jet towards S5, reacting with PbLi in the expansion vessel, and affects the water fragmentation, diminishing the interfacial area, therefore the interaction, between fluids.

From the quantitative accuracy evaluation point of view, considering the peculiarity of LIFUS5 Tests# transient, their execution, and the availability of experimental data, the quantitative evaluation of the results accuracy has been performed on the pressures of reaction and expansion vessels. The results of the reference calculation for all the analyzed Test# are reported in Table 8. DEV2_SIGN is positive for all the calculations, confirming that the code over-predicts the experimental results. The application of the FFTBM at cut frequencies of 100 Hz leads to reasonable values of the average amplitude, in particular for Test#6 (S1 pressure), Test#7 and Test#8 (there is a clear evidence that the code results are affected by the correct knowledge of tests boundary conditions as mentioned before). Indeed, in these tests, PT3 was installed in the injection line, and its experimental trend was imposed as BIC, while a postulated time trend was assumed for Tests#3-5. The quantitative accuracy evaluation of S5 pressure in T#6 is not reliable due to abnormal experimental pressure recorded by PT1 (Refs. [7], [33]).

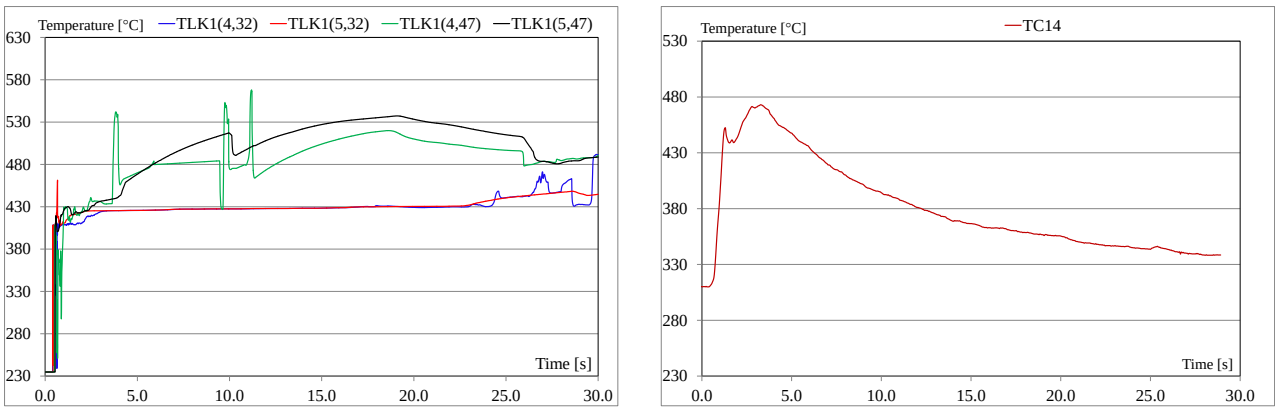

Fig. 11. T#8: CALC results (left) of PbLi temperature trends in S5 vs EXP data (right).

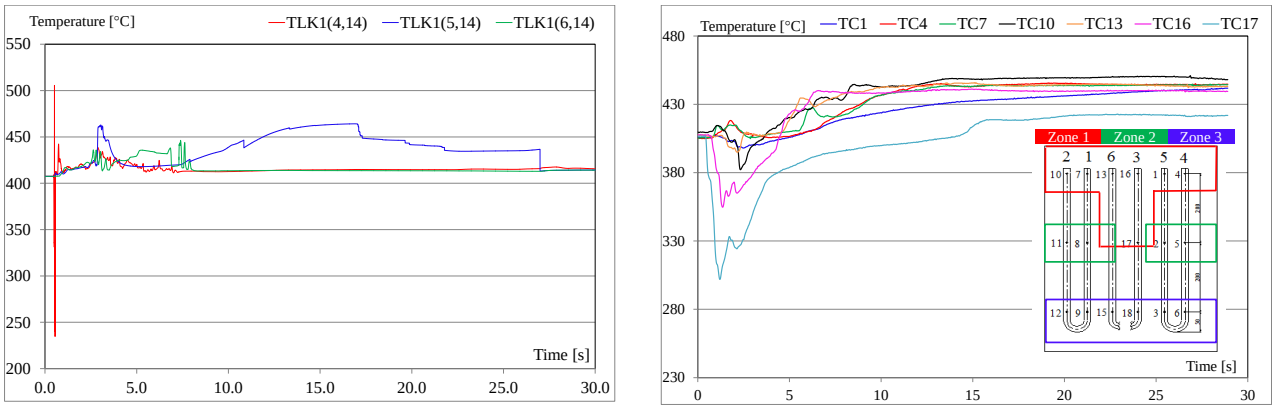

Fig. 12. T#8: CALC results (left) of PbLi temperature trends in S1 vs EXP data (right).– zone 1.

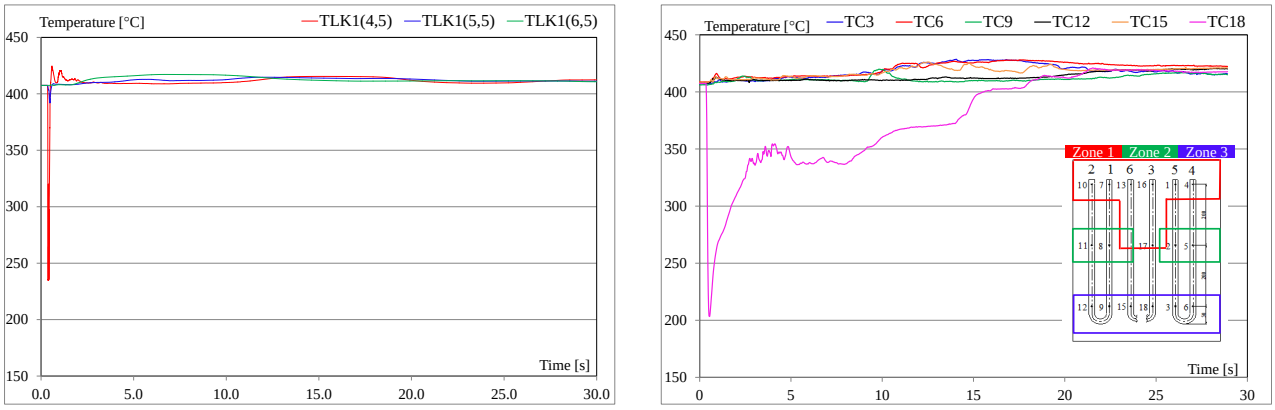

Fig. 13. T#8: CALC results (left) of PbLi temperature trends in S1 vs EXP data (right). – zone 3.

Table 3. T#8 RUN0: comparisons between measured and calculated initial condition results.

#	Parameter	Unit	EXP [ID]	Design Value	EXP Value	CALC Value	Avg Error
1	Abs. Pressure in S1	bar	--	NA	NA	1	-- %
2	PbLi temperature in S1	°C	TC7-TC2	430	406÷409	407	0 °C
3	Water temperature in injector	°C	--	320	NA	327	-- °C
4	Gas temperature in S5	°C	TC14	NA	311	310	1 °C
5	Abs. Pressure in injection zone(1)	bar	PT3	vacuum	NA	1	%
6	Free volume in S1+S5	m^3	--	0.0155	NA	0.0156	-- %

(1) The injection zone is defined as the volume between the injection valve and the cap, where vacuum is done

Table 4. T#8 RUN0: thermal-hydraulic condition of water at the injection time.

#	Conditions	Value	Note
1	Pressure at the injector	50.4 bar	The TH conditions are calculated by the code @ t = 334 ms after SoT
2	Temperature of injected water	267.3 °C	
3	Void fraction of two-phase conditions	0.892	

Table 5. T#8 RUN0: phenomenological analysis

#	Phase	Time span [ms]
0	Water injection line pressurization	0 – 334
1	Coolant flashing and reaction vessel pressurization	334 – 680
2	Expansion volume pressurization	680 – 1530
3	S1 and S5 pressures equilibrium	1530 – 11777
4	System pressure stabilization	11777 – EoT

Table 6. T#8 RUN0: resulting sequence of main events.

#	Event	EXP [ms]	CALC [ms]	Note
1	Start of transient (V14 opening signal)	0	0	-
2	Vacuum line pressurization	SoT-334	SoT-334	Imposed as BIC
3	Injector breaking-up	334	334	Start of Phase 1
4	Water flashing and first pressure peak	337	336	-
5	Gas flowing in expansion tubes	NA	490	-
6	S5 start pressurization	680	530	End of Phase 1
7	S1 and S5 pressure equilibrium	1530	2100	End of Phase 2
8	Water end injection	4100	2700	EXP datum based on system pressure trend
9	V14 closing signal	11777	11777	End of Phase 3

Table 7. T#8 RUN0: parameters characterizing the RTA.

QUALITATIVE ACCURACY EVALUATION		UNIT	EXP	CALC	JUDG
RTA: WATER INJECTION BEHAVIOR					
TSE	Injector break-up	ms	334	334	E
	Time of onset of subcooled injection	ms	NA	474	--
	Time of stop injection (mass flow rate negligible)	ms	NA	2700	--
	Time of End of Ph1	ms	680	530	R
	Time of End of Ph2	ms	1530	2100	M
	Time of End of Ph3	ms	11777	11777	E
SVP	T of injection – Tsat @ injector break-up	°C	NA	0.0	--
	Mass flow rate @ first pressure peak	kg/s	NA	0.35	--
	Mass flow rate @ onset of subcooled injection	kg/s	NA	0.78	--
	Mass flow rate @ EoPh1	kg/s	NA	0.67	--
	Mass flow rate @ EoPh2	kg/s	NA	0.25	--
	Mass flow rate @ EoPh3	kg/s	NA	0.00	--
	Pressure of injection line @ break-up	bar	50.78	50.43	E
	Pressure of injection line @ onset of subcooled injection	bar	NA	133.7	--
	Pressure of injection line @ EoPh1	bar	140.0	138.6	E
	Pressure of injection line @ EoPh2	bar	139.8	142.1	E
	Pressure of injection line @ EoPh3	bar	160.4	159.0	E
IPA	Integral mass flow rate @ first pressure peak	g	NA	0.7	--
	Integral mass flow rate @ onset of subcooled injection	g	NA	81.9	--
	Integral mass flow rate @ EoPh1	g	NA	122.2	--
	Integral mass flow rate @ EoPh2	g	NA	803.6	--
	Integral mass flow rate @ EoPh3	g	NA	939.9	--
NDP	Void fraction @ injector break-up	--	NA	0.892	--
RTA: REACTION VESSEL PRESSURE BEHAVIOR					
TSE	Time of first pressure peak due to water flashing in S1	ms	347	346	E
	Time of 10% total mass flow rate	ms	NA	484	--
	Time of 50% total mass flow rate	ms	NA	1140	--
	Time of 80% total mass flow rate	ms	NA	1893	--
	Time of 100% total mass flow rate	ms	NA	9721	--

SVP	Water flashing – first pressure peak	bar	4.7	7.9	R
	S1 pressure @ EoPh1	bar	38.9	44	R
	Pressure increase rate from 0s to EoPh1	bar/s	111	214	M
	S1-S5 pressure equilibrium @ EoPh2	bar	86.5	129.3	M
	S1-S5 pressures @ EoPh3	bar	150.2	160.0	R
RTA: EXPANSION VESSEL PRESSURE BEHAVIOR					
TSE	Time of onset S5 pressurization	ms	680	530	R
	Time of max PbLi mass in S5	ms	NA	2665	--
SVP	Pressure increase rate during Ph2	bar/s	55.4	78.9	R
	Gas volume in S1+S5 @ SoT - IMPOSED	m^3	NA	0.0156	--
	PbLi mass in S5 @ onset of pressurization	kg	NA	0.85	--
	PbLi mass in S5 @ EoPh2	kg	NA	42.67	--
	PbLi mass in S5 @ EoPh3	kg	NA	20.25	--
	Max PbLi mass in S5 during the transient	kg	NA	45.10	--
NDP	Gas volume in S5 @ onset of pressurization / Gas volume @ SoT	--	NA	0.99	--
	Gas volume in S5 @ EoPh2 / Gas volume @ SoT	--	NA	0.49	--
	Gas volume in S5 @ EoPh3 / Gas volume @ SoT	--	NA	0.75	--
	Min gas volume in S5 / Gas volume @ SoT	--	NA	0.46	--
RTA: FLOW BEHAVIOR IN EXPANSION TUBES					
TSE	Time of onset of PbLi mass flow in expansion tubes	ms	NA	341	--
	Time of max PbLi mass flow rate	ms	NA	424	--
	Time of end of PbLi mass flow rate towards S5	ms	NA	2645	--
	Time of onset of water mass flow rate	ms	NA	525	--
	Time of max vapor mass flow rate	ms	NA	637	--
	Time of onset of gases mass flow rate	ms	NA	490	--
	Time of max gas mass flow rate	ms	NA	596	--
SVP	Max PbLi mass flow rate in expansion tubes from 0s to EoPh2	kg/s	NA	49.7	--
	Max gas mass flow rate from onset to EoT	kg/s	NA	0.148	--
	Max vapor mass flow rate from onset to EoT	kg/s	NA	0.245	--
RTA: CHEMICAL REACTION INTERACTION					
TSE	Time of onset of H_2 production	ms	NA	335	--
	Time of end of H_2 linear generation	ms	NA	2455	--
	Time of onset constant H_2 inventory	ms	NA	9220	--
	Time of maximum PbLi temperature in S1	ms	13700	517	M
	Time of maximum PbLi temperature in S5	ms	3270	3816	R
	Time of minimum PbLi temperature in S1	ms	511	478	R
SVP	Max PbLi temperature in S1	°C	450	506	M
	Min PbLi temperature in S1	°C	204	235	R
	Max PbLi temperature in S5	°C	473	542	M
	PbLi average temperature in S1 zone 1 @ EoT	°C	440	416	M
	PbLi average temperature in S1 zone 2 @ EoT	°C	420	415	R
	PbLi average temperature in S1 zone 3 @ EoT	°C	419	411	R
	PbLi average temperature in S5 @ EoT	°C	338	479	M
	PbLi mass inventory @ SoT - IMPOSED	kg	NA	960.79	--
	PbLi mass inventory @ EoT	kg	NA	959.73	--
	Mass of subcooled water in system @ EoT	kg	NA	0.0	--
	Mass of water vapor in system @ EoT	g	NA	0.192	--
	H_2 linear generation rate @ EoPh2	g/s	NA	36.7	--
IPA	Integral H_2 production @ first pressure peak	g	NA	0.0	--
	Integral H_2 production @ EoPh1	g	NA	6.7	--
	Integral H_2 production @ EoPh2	g	NA	64.9	--
	Integral H_2 production @ EoPh3	g	NA	76.4	--
	Integral H_2 production @ EoT	g	NA	76.4	--

Table 8. Quantitative accuracy evaluation results.

#	Parameter	EXP-CALC	$DEV2_{SIGN}$	$DEV2_{ABS}$	$DEV2_{RMS}$	AA	WF
T#3	Pressure S1	PT5-PK[6,8][(1)]	15.15	15.24	17.25	0.21	8.34
	Pressure S5	PT1-PK[6,54][(1)]	14.71	14.94	17.76	0.28	9.49
T#4	Pressure S1	PT5-PK[6,7]	8.38	11.60	15.20	0.35	14.39
	Pressure S5	PT1-PK[5,47]	12.82	12.86	18.72	0.57	12.29
T#5	Pressure S1	PT5-PK[6,7]	7.32	9.79	12.48	0.30	9.82
	Pressure S5	PT1-PK[5,47]	6.09	6.99	0.02	0.32	17.57
T#6	Pressure S1	PT5-PK[6,7]	14.62	14.82	15.85	0.16	10.58
	Pressure S5	PT1-PK[5,47]	70.43	70.43	77.03	0.97	8.22
T#7	Pressure S1	PT5-PK[6,7]	13.10	13.19	14.27	0.15	10.97
	Pressure S5	PT1-PK[5,47]	15.34	15.34	21.70	0.27	4.28
T#8	Pressure S1	PT5-PK[6,7]	14.23	14.23	15.03	0.15	9.00
	Pressure S5	PT1-PK[5,47]	10.44	10.49	11.43	0.13	9.01

(1) The reference mesh cells are different due to modified input deck of T#3

Table 9: LIFUS5 Test#8: sensitivity calculation matrix

ID	P inj	T H_2O [K]	FMOL	FKCR	GAS S1+S5 [m^3]	Nodalization	Objectives
RUN#0 (Reference)	as PT3	600.15	0.75	0.1	0.0156	only tubes	Reference calculation
RUN#1	as Run0	**610.15**	0.75	0.1	0.0156	only tubes	To analyze the influence of imperfect knowledge of BIC
RUN#2	as Run0	**590.15**	0.75	0.1	0.0156	only tubes	
RUN#3	as Run0	600.15	**1**	0.1	0.0156	only tubes	To analyze the code response on the chemical implemented models and optimize the results
RUN#4	as Run0	600.15	0.75	**0.001**	0.0156	only tubes	
RUN#5	as Run0	600.15	0.75	0.1	**0.0111**	only tubes	To investigate the influence of BIC on the code results reliability
RUN#6	as Run0	600.15	0.75	0.1	**0.0201**	only tubes	
RUN#7	as Run0	600.15	0.75	0.1	0.0156	**with elbow**	To investigate the effect of user choices and modeling on code results
RUN#8	as Run0	600.15	0.75	0.1	0.0156	**different mock-up**	

5.3. Sensitivity calculations

Sensitivity analyses (step 3) are performed for each Test#. Considering T#8, a total of 8 sensitivity calculations are performed starting from RUN#0_Reference (Table 9):

- RUN#1-RUN#2 (Fig. 14). The temperature of the injected water has been changed in order to analyze the influence of the imperfect knowledge of boundary and initial conditions. Only slight differences occur during the transient. The first pressure peak due to water flashing is affected by the temperature of the injected water. The pressure peak occurs at the same time of 336 ms and varies from 7.0 bar (Run#1) to 8.0 bar (Run#2). The reference calculation predicts a pressure peak due to water flashing of 7.9 bar. Indeed, lower is the temperature of the injected water, higher the subcooling rate, so higher the density and higher the water mass flow rate (and thus the total mass inside S1) and therefore higher is the pressurization of S1 due to water vaporization and flashing. The pressurization rate of S1 during Phase 1 is only marginally affected by the injected water temperature. On the other hand, this parameter influences the S5 pressurization rate, probably due to a combined effect of the jet-breaking modeling, between 900 ms and the S1-S5 equilibrium. Indeed, since the jet-breaking is not simulated, the water is easily injected towards S5 expansion vessel. If the temperature of the water is higher (Run#1), its expansion in S1 reaction vessel is lower, and the water can reach the expansion vessel and here it vaporizes, increasing the pressure.

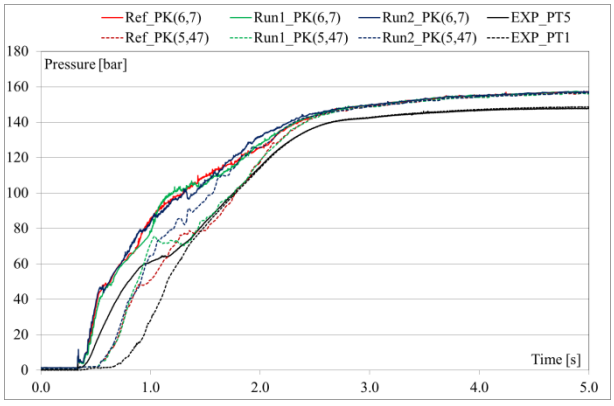

Fig. 14. T#8 sensitivity analyses: influence of temperature. CALC pressure in S1 PK(6,7) and in S5 PK(5,47) vs EXP data.

- RUN#3-RUN#4 (Fig. 15). Two code parameters which influence the chemical model implemented in the code are selected as parameters to analyze the code response and optimize the results. They are FMOL and FKCR, which represent respectively the conversion ratio of water into hydrogen in the chemical reactions and the constant of hydrogen generation reaction (mol/m4/s). Run#3 and Run#4 show the same pressure peak due to water flashing as the reference calculation, but the sensitivities predict also a secondary pressure peak at 342 ms of 15.7 bar (Run#3) and 16.8 bar (Run#4). During Phase 1, Run#3 shows a faster reaction vessel pressure increase, followed by a suddenly decrease once the onset of S5 pressurization occurs. The pressurization rate of S1 and S5 are faster also during Phase 2. The trend is coherent with the chemical model applied since FMOL equal to 1 means that SIMMER code predicts a greater amount of hydrogen generation (Ref. [6]). Therefore, the equilibrium between S1 and S5 is reached earlier at about 1255 ms and at a pressure of 92.5 bar. Run#4 shows qualitative better results of pressure in the reaction vessel. The pressurization rate during Phase 1 is in line with the experimental trends (slightly faster), as well as the changing slope. The behavior is still anticipated in time due to the influence of jet fragmentation. The onset of S5 expansion vessel pressurization is anticipated and therefore Phase 1 and Phase 2 end earlier.

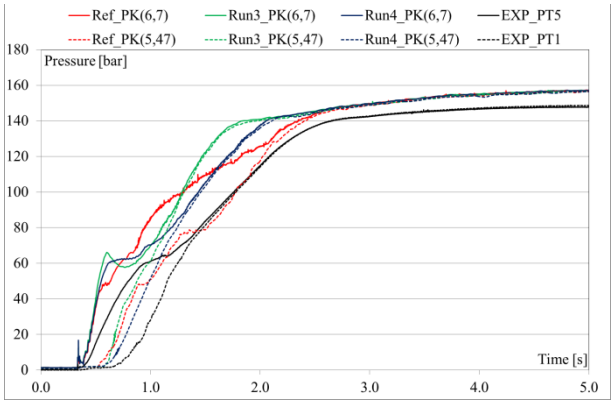

Fig. 15. T#8 sensitivity analyses: influence of chemical parameters. CALC pressure in S1 PK(6,7) and in S5 PK(5,47) vs EXP data.

- RUN#5-RUN#6 (Fig. 16). The free gas volume in S1 has been changed to investigate the influence of boundary and initial conditions on the code results reliability. The pressurization rate of the reaction vessel changes accordingly with the volume of free gas. Run#5 (lower free gas) shows a pressure peak in S1, followed by a pressure decrease when the onset of S5 pressurization occurs, while Run#6 (greater free gas) shows a smoother pressure increase. The gas volume affects also Phase 2 and the S5 pressurization behavior. The equilibrium between S1 and S5 is reached at about 2035 ms and 138 bar for Run#5, while for Run#6 it occurs anticipated in time and at lower pressure value (1260 ms and 82 bar). Phase 3 is not affected by the volume of the free gas in the system.

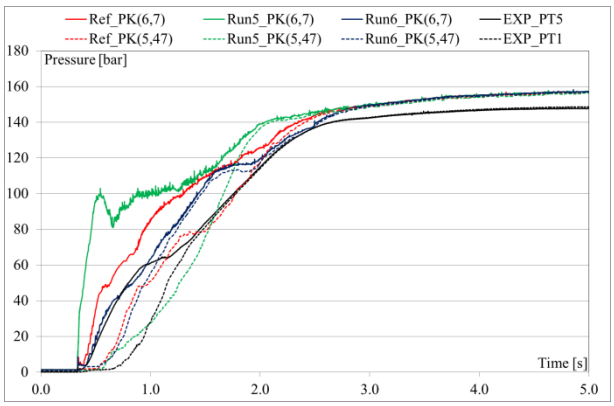

Fig. 16. T#8 sensitivity analyses: influence of gas volume. CALC pressure in S1 PK(6,7) and in S5 PK(5,47) vs EXP data.

- RUN#7-RUN#8 (Fig. 17). The sensitivity calculations investigate the nodalization effect on the code results, particularly the modeling of the elbow curves of U-tubes which are responsible to break the water jet and the U-tube modeling on the PbLi temperature effects. The first pressure peak due to water flashing is higher in the sensitivity calculations due to higher fragmentation and vaporization. It varies from 6.8 bar (reference calculation) to 7.5 bar (Run#7) and to 9.1 bar (Run#8). Phase 1 is strongly influenced by the jet-fragmentation modeling, because S5 pressurization largely varies. Run#7 shows the onset of S5 pressurization at about 1310 ms. As a consequence, the S1 pressure shows an increase and then it stabilizes at about 100 bar up to about 1800 ms. Then, it increases again up to about 1950 ms, when the S1 and S5 pressures are equalized (110 bar). Run#8 shows a S1 pressure behavior similar to Run#7, however the onset of S5 pressurization is slightly anticipated and the pressurization rate is faster. As a matter of that, the equilibrium between S1 and S5 occurs earlier but at higher pressure value (120 bar and 1640 ms). The phenomenology connected with the S5 pressurization during Phase 2 (time of start pressurization and rate of pressurization) is affected by the water jet breaking. Indeed, in Run#7 and Run#8, the water injected in S1 reaction vessel immediately is fragmented and evaporates. Then, the gases and vapor trapped in the U-tube sector push the PbLi through the expansion tubes, and the S5 expansion vessel becomes a quasi-solid system. It is calculated a percentage of 13.7% and 6.2% of free gas in S5 during the transient, respectively for Run#7 and Run#8. This condition does not allow the gas mass flow rate through the expansion tubes. The sudden S5 pressurization, due only to the “piston effect” of the PbLi, corresponds to this time. The temperature trends (Fig. 18) are affected by the jet-fragmentation modeling and by the nodalization. The reference calculation shows higher temperature values in S5 (the average value at the EoT is 479°C against the experimental value of 338°C), while these temperatures in Run#7 and Run#8 show a peak when the liquid metal reaches the expansion vessel S5, and then they rapidly decrease, clear evidence that the chemical reaction is enclosed in S1 reaction vessel. This behavior reflects the phenomenology of the transient.

The sensitivity results underline the importance of the correct knowledge of initial and boundary conditions (the temperature of the injected water, the free gas volume in the expansion vessel, as shown in Fig. 14 and Fig. 16). Moreover, the results show that such kind of interaction phenomena is extremely complex to simulate because affected by a large number of parameters (i.e. interfacial area, dimensions of the vapor bubble, heat transfer coefficient, fragmentation model due to the jet-breaking, see Fig. 17 and Fig. 18).

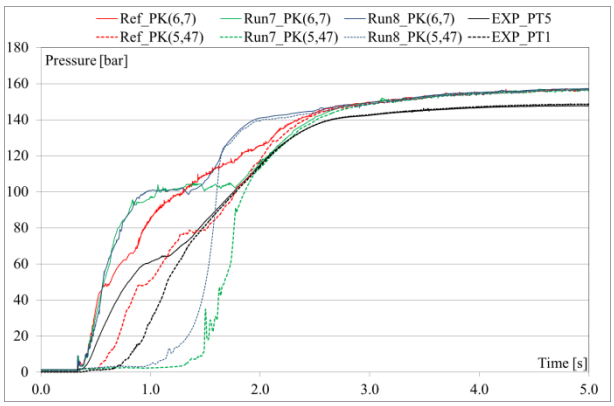

Fig. 17. T#8 sensitivity analyses: influence of nodalization. CALC pressure in S1 PK(6,7) and in S5 PK(5,47) vs EXP data.

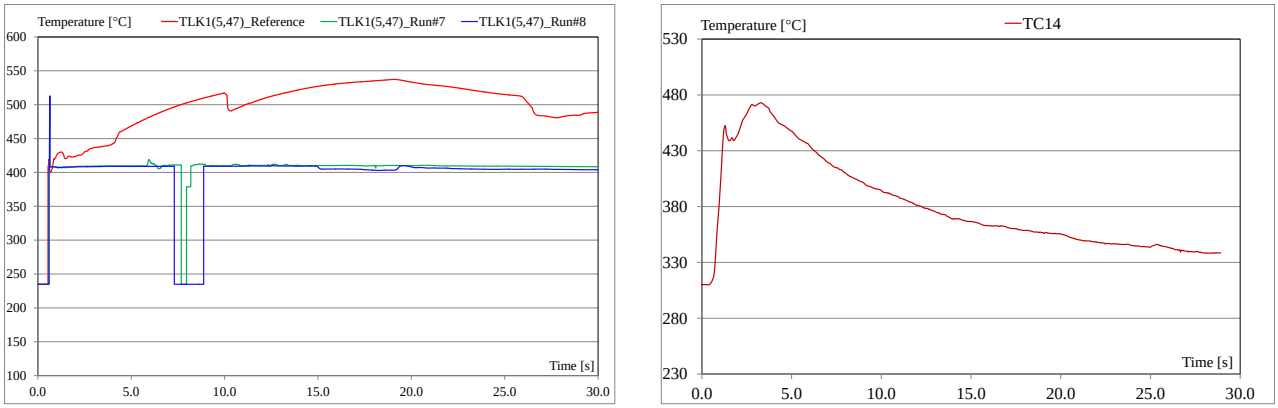

Fig. 18. T#8 sensitivity analyses: influence of nodalization. CALC results (left) of PbLi temperature trends in S5 vs EXP data (right).

6. Conclusions

The objective of the paper is to assess the modified version of SIMMER-III code in predicting WCLL BB "in-box-LOCA" scenario, describing the performances of the code simulations and its capability to reproduce the relevant thermal-hydraulic phenomena during PbLi/water interaction, including the chemical reaction.

The objective is fulfilled through comprehensive comparisons based on the following steps:

- Description of LIFUS5 facility and experimental campaign, highlighting the knowledge of the tests execution and the open issues;
- Description of reference LIFUS5 nodalization by SIMMER-III code, the applied initial and boundary conditions, and the modified input deck;
- Assessment of SIMMER-III code applying a standard code validation methodology against all tests of LIFUS5 experimental campaign. The methodology is based on three-step approach as a part of the code assessment process:
  - Step 1: Initial condition results at injection time, relevant for the characterization of the thermal-hydraulic conditions at the beginning of the experiment;
  - Step 2: Reference calculation results, based on the comparison between measured and calculated trends or values and performed through qualitative and quantitative evaluations;
  - Step 3: Results from sensitivity analyses, performed in order to investigate the robustness of the code results and to evaluate the relevance of selected parameters and/or user choices.

The analysis of the results demonstrates the following:

- The initial conditions results highlight that during the vacuum line pressurization, an early rupture of the injector cap occurred, leading to two-phase injection conditions. The calculations permit to improve the knowledge of tests procedure and tests operating conditions;
- The modified version of SIMMER-III code for fusion application is able to predict the relevant thermal-hydraulic phenomena during PbLi/water interaction (i.e. pressure trends due to water flashing and evaporation and due to hydrogen generation);
- The temperature trends evidence that the exothermic chemical reaction between PbLi and water is reasonably simulated, although the chemical energy is derived from the TC measurements;
- Most of all the sensitivities pointed out the relevance of the initial and boundary conditions on the predictive capabilities of SIMMER-III code to

simulate phenomena connected with lithium-lead/water interaction;

- The code simulations of Tests#6-8 have an average amplitude of S1 pressure equal or lower than 0.16, confirming the importance of the correct knowledge of initial and boundary conditions in code predicting capabilities;
- All code simulations showed a good prediction of the experiment, i.e. AA lower than 0.35 for S1 pressure. The result of AA is higher for S5 pressure in Test#6 due to abnormal experimental pressure recorded by PT1.

In conclusion, the present activity brought to the following achievements:

- The code has demonstrated promising capability in predicting phenomena connected with lithium-lead and water interaction, considering also the chemical reaction and hydrogen production.
- The activity contributed to the SIMMER-III code accuracy quantification, helping identifying most accurate code results, code models, and helping in experimental test comprehension.
- The code validation activity is ongoing, and will be conducted applying the methodology once qualified data (i.e. pressures, temperatures, amount of injected water, and hydrogen production quantification) will be provided by next LIFUS5/Mod3 campaign, executed with controlled and well-known initial and boundary conditions.

Nomenclature

Avg	Average
BB	Breeding Blanket
BIC	Boundary and Initial Condition
CALC	Calculated
CR	Research Center
DEMO	DEMOnstration Fusion Reactor
DSA	Deterministic Safety Analysis
DWT	Double Wall Tube
E	Excellent
EDTAR	Experimental Data Test and Analysis Report
EoPh	End of Phase
EoT	End of Transient
ESF	Engineering Safety Function
EXP	Experimental
FFTBM	Fast Fourier Transform Based Method
I&B	Initial and Boundary
IPA	Integral PArameter
JUDG	Judgment
LOCA	Loss Of Coolant Accident
M	Minimal
NA	Not Available
NDP	Non-Dimensional Parameter
PbLi	Lithium lead
PK	Pressure (SIMMER nomenclature)
PIE	Postulated Initial Event
PT	Pressure Transducer
R	Reasonable
RTA	Relevant Thermal-hydraulic Aspect
SoT	Start of Transient
SVP	Single Valued Parameter
TBA	To Be Assessed
TC	Thermo-Couple
TLK1	PbLi temperature (SIMMER nomenclature)
TSE	Time Sequence of Events
U	Unqualified
WCLL	Water Cooled Lithium Lead

Acknowledgments

This work has been carried out within the framework of the EUROfusion Consortium and has received funding from the Euratom research and training programme 2014-2018 and 2019-2020 under grant agreement No 633053. The views and opinions expressed herein do not necessarily reflect those of the European Commission.

References

[1] E. Martelli et al., *Advancements in DEMO WCLL breeding blanket design and integration,* Int. J. Energy Res. (2017), https://doi.org/10.1002/er.3750.

[2] A. Del Nevo et al., *WCLL breeding blanket design and integration for DEMO 2015: status and perspectives*, Fusion Eng. Des. Volume 124, November 2017, Pages 682-686, https://doi.org/10.1016/j.fusengdes.2017.03.020.

[3] G. Federici et al., *An overview of the EU breeding blanket design strategy as an integral part of the DEMO design effort*, Fusion Eng. Des., Volume 141, April 2019, Pages 30-42, https://doi.org/10.1016/j.fusengdes.2019.01.141.

[4] M. Eboli, et al., *Simulation study of pressure trends in the case of loss of coolant accident in Water Cooled Lithium Lead blanket module*, Fusion Eng. Des. Volumes 98–99, October 2015, Pages 1763-1766, https://doi.org/10.1016/j.fusengdes.2015.05.034.

[5] IAEA, *Accident Analysis for Nuclear Power Plant, Safety Reports Series, no.23*, Austria, Nov. 2002, ISBN 92–0–115602–2.

[6] M. Eboli, N. Forgione, A. Del Nevo, *Implementation of the chemical PbLi/water reaction in the SIMMER code*, Fusion Eng. Des. Volumes 109–111, Part A, 1 November 2016, Pages 468-473, https://doi.org/10.1016/j.fusengdes.2016.02.080.

[7] M. Eboli, *Safety Investigation of in-box LOCA for DEMO Reactor: Experiments and Analyses*, PhD thesis, June 2017, https://etd.adm.unipi.it/theses/available/etd-05302017-093203.

[8] M. Eboli, et al., *Experimental activities for in-box LOCA of WCLL BB in LIFUS5/Mod3 facility*, Fusion Eng. Des., Volume 146, Part A, September 2019, Pages 914-919, https://doi.org/10.1016/j.fusengdes.2019.01.113.

[9] M. Eboli, et al., *Test Series D experimental results for SIMMER code validation of WCLL BB in-box LOCA in LIFUS5/Mod3 facility*, Fusion Eng. Des., Volume 156, July 2020, 111582, https://doi.org/10.1016/j.fusengdes.2020.111582

[10] S. Khani et al., *Validation of SIMMER-III code for in-box LOCA of WCLL BB: pre-test analysis of Test D1.1 in LIFUS5/Mod3 facility*, Fusion Eng. Des., Volume 146, Part A, September 2019, Pages 978-982, https://doi.org/10.1016/j.fusengdes.2019.01.131.

[11] S. Khani, et al., *Analysis of Test D1.1 of the LIFUS5/Mod3 facility for In-box LOCA in WCLL-BB*, Fusion Eng. Des., Volume 160, November 2020, 111832, https://doi.org/10.1016/j.fusengdes.2020.111832

[12] K. Umminger, A. Del Nevo, *Integral Test Facilities and Thermal-Hydraulic System Codes in Nuclear Safety Analysis*, Science and Technology of Nuclear Installations, vol. 2012, Article ID 826732, 3 pages, 2012.

[13] B. Gonfiotti, et al., *Development of a SIMMER\RELAP5 coupling tool*, Fusion Eng. Des., Volume 146, Part B, September 2019, Pages 1993-1997, https://doi.org/10.1016/j.fusengdes.2019.03.084.

[14] F. Galleni, et al., *RELAP5/SIMMER-III code coupling development for PbLi-water interaction*, Fusion Eng. Des., Volume 153, April 2020, 111504, https://doi.org/10.1016/j.fusengdes.2020.111504

[15] F. D'Auria, G. M. Galassi, *Code assessment methodology and results*, IAEA Technical Workshop/Committee on Computer Aided Safety Analyses, Moscow, May 14-17, 1990.

[16] M. Bonuccelli, F. D'Auria, N. Debrecin, G. M. Galassi, *A Methodology for the Qualification of Thermalhydraulic Code Nodalizations*, Proc. of NURETH-6 Conference, Grenoble (F), October 5-8, 1993.

[17] D'Auria F., G. M. Galassi, *Code Validation and Uncertainties in System Thermal-hydraulics*, J. Progress in Nuclear Energy, Vol. 33 Nos. 1&2, 1998, pages 175-216.

[18] F. D'Auria, C. Camargo, O. .Mazzantini, *The Best Estimate Plus Uncertainty (BEPU) approach in licensing of current nuclear reactors*, Nuclear Eng. Des. Volume 248, July 2012, Pages 317-328. https://doi.org/10.1016/j.nucengdes.2012.04.002

[19] R.F Kunz, G.F. Kasmala, J.H. Mahaffy, C.J. Murray, *On the Automated Assessment of Nuclear Reactor Systems Code Accuracy*, Nuclear Eng, Des., Volume 211, Issues 2–3, February 2002, Pages 245-272, https://doi.org/10.1016/S0029-5493(01)00440-X

[20] F. D'Auria, A. Bousbia-Salah, A. Petruzzi, A. Del Nevo, *State of the Art in Using Best Estimate Calculation Tools in Nuclear Technology*, Nuclear Engineering and Technology, Vol. 38, No. 1, Feb. 2006, pp 11-32.

[21] F. Moretti, et al., *CFD Analysis of a Slug Mixing Experiment Conducted on a VVER-1000 Model*, Science and Technology of Nuclear Installations, vol. 2009, Article ID 436218, 12 pages, 2009.

[22] U. Rohde, T. Höhne, S. Kliem et al., *Fluid mixing and flow distribution in a primary circuit of a nuclear pressurized water reactor—Validation of CFD codes*, Nuclear Eng, Des., Volume 237, Issues 15–17, September 2007, Pages 1639-1655, https://doi.org/10.1016/j.nucengdes.2007.03.015.

[23] W. Ambrosini, R. Bovalini, F. D'Auria, *Evaluation of accuracy of Thermal-hydraulic code calculations*, J. Energia Nucleare, Vol. 2, 1990.

[24] Aksan S. N., F. D'Auria, H. Staedtke, *User Effects on the Thermal-hydraulic Transient System Codes Calculations*, Nucl. Eng. Des., Volume 145, Issues 1–2, 2 November 1993, Pages 159-174, https://doi.org/10.1016/0029-5493(93)90065-H.

[25] A. Ciampichetti, et al., *Water large leaks into liquid Pb-17Li: first experimental results on LIFUS 5 facility*, Fusion Eng. Des. Volume 69, Issues 1–4, September 2003, Pages 563-567, https://doi.org/10.1016/S0920-3796(03)00135-2.

[26] A. Ciampichetti, et al., *Pb-16Li/water interaction: Experimental results and preliminary modelling activities*, Fusion Eng. Des. Volume 88, Issues 9–10, October 2013, Pages 2392-2395. https://doi.org/10.1016/j.fusengdes.2013.05.039.

[27] L. Giancarli, M. Dalle Donne, W. Dietz, *Status of the European breeding blanket technology*, Fusion Eng. Des. Volume 36, Issue 1, April 1997, Pages 57-74. https://doi.org/10.1016/S0920-3796(97)00012-4.

[28] M. Eboli, A. Del Nevo, N. Forgione, M. T. Porfiri, *Post-Test Analyses of LIFUS5 Test#3 Experiment*, Fusion Eng. Des., Volume 124, November 2017, Pages 856-860. https://doi.org/10.1016/j.fusengdes.2017.03.046.

[29] AA.VV., *SIMMER-III (Version 3.F) Input Manual*, O-arai Engineering Center, Japan Nuclear Cycle Development Institute, May 2012.

[30] M. Eboli, N. Forgione, A. Del Nevo, SIMMER-III Ver.3F Mod.0.1 validation against LIFUS5 Test#3 experiment, DM-D-R-241, 16 January 2017.

[31] M. Eboli, N. Forgione, A. Del Nevo, SIMMER-III Ver.3F Mod.0.1 validation against LIFUS5 Test#4 experiment, DM-D-R-247, 23 January 2017.

[32] M. Eboli, N. Forgione, A. Del Nevo, SIMMER-III Ver.3F Mod.0.1 validation against LIFUS5 Test#5 experiment, DM-D-R-248, 07 February 2017.

[33] M. Eboli, N. Forgione, A. Del Nevo, SIMMER-III Ver.3F Mod.0.1 validation against LIFUS5 Test#6 experiment, DM-D-R-249, 13 February 2017.

[34] M. Eboli, N. Forgione, A. Del Nevo, SIMMER-III Ver.3F Mod.0.1 validation against LIFUS5 Test#7 experiment, DM-D-R-250, 20 February 2017.

[35] M. Eboli, N. Forgione, A. Del Nevo, SIMMER-III Ver.3F Mod.0.1 validation against LIFUS5 Test#8 experiment, DM-D-R-251, 20 February 2017.